

Upconversion luminescence, intensity saturation effect, and thermal effect in Gd₂O₃:Er³⁺,Yb³⁺ nanowires

Yanqiang Lei, Hongwei Song, Linmei Yang, Lixin Yu, Zhongxin Liu et al.

Citation: *J. Chem. Phys.* **123**, 174710 (2005); doi: 10.1063/1.2087487

View online: <http://dx.doi.org/10.1063/1.2087487>

View Table of Contents: <http://jcp.aip.org/resource/1/JCPSA6/v123/i17>

Published by the [American Institute of Physics](#).

Additional information on J. Chem. Phys.


Journal Homepage: <http://jcp.aip.org/>

Journal Information: http://jcp.aip.org/about/about_the_journal

Top downloads: http://jcp.aip.org/features/most_downloaded

Information for Authors: <http://jcp.aip.org/authors>

ADVERTISEMENT



AIPAdvances

Special Topic Section:
PHYSICS OF CANCER

Why cancer? Why physics? [View Articles Now](#)

Upconversion luminescence, intensity saturation effect, and thermal effect in $\text{Gd}_2\text{O}_3:\text{Er}^{3+}, \text{Yb}^{3+}$ nanowires

Yanqiang Lei, Hongwei Song,^{a)} Linmei Yang, Lixin Yu, Zhongxin Liu, Guohui Pan, Xue Bai, and Libo Fan

Key Laboratory of Excited State Physics, Changchun Institute of Optics, Fine mechanics and Physics, Chinese Academic of Sciences, Changchun 130033, People's Republic of China

(Received 26 April 2005; accepted 1 September 2005; published online 3 November 2005)

In this paper, the upconversion luminescent properties of $\text{Gd}_2\text{O}_3:\text{Er}^{3+}, \text{Yb}^{3+}$ nanowires as a function of Yb concentration and excitation power were studied under 978-nm excitation. The results indicated that the relative intensity of the red emission (${}^4F_{9/2}-{}^4I_{15/2}$) increased with increasing the Yb^{3+} concentration, while that of the green emission (${}^4S_{3/2}/{}^2H_{11/2}-{}^4I_{15/2}$) decreased. As a function of excitation power in \ln - \ln plot, the green emission of ${}^4S_{3/2}-{}^4I_{15/2}$ yielded a slope of ~ 2 , while the red emission of ${}^4F_{9/2}-{}^4I_{15/2}$ yielded a slope of ~ 1 . Moreover, the slope decreased with increasing the Yb^{3+} concentration. This was well explained by the expanded theory of competition between linear decay and upconversion processes for the depletion of the intermediate excited states. As the excitation power density was high enough, the emission intensity of upconversion decreased due to thermal quenching. The thermal effect caused by the exposure of the 978-nm laser was studied according to the intensity ratio of ${}^2H_{11/2}-{}^4I_{15/2}$ to ${}^4S_{3/2}-{}^4I_{15/2}$. The practical sample temperature at the exposed spot as a function of excitation power and Yb^{3+} concentration was deduced. The result indicated that at the irradiated spot ($0.5 \times 0.5 \text{ mm}^2$) the practical temperature considerably increased. © 2005 American Institute of Physics. [DOI: 10.1063/1.2087487]

I. INTRODUCTION

Recently, much attention has been given to trivalent rare-earth (RE^{3+})-doped phosphors with particle sizes in the nanometer region.¹⁻⁴ The reduction of particle size of crystal-line systems may lead to important modifications of some of their bulk properties, such as higher luminescent efficiency and better resolution of images in lighting and display.⁵ So far, many RE-doped nanocrystalline (NC) systems have been prepared using various synthesis procedures and their luminescent properties have been widely studied.⁶⁻⁹

Following the availability of near-infrared (NIR) pump sources, such as solid-state lasers and semiconductor laser diodes, NIR to visible upconversion luminescence (UCL) has garnered significant attention. Among the candidates of upconversion materials, tripositive erbium (Er^{3+}) has excellent upconversion properties.¹⁰⁻¹² In the NIR region, Er^{3+} has a favorable energy-level structure with two transitions ${}^4I_{15/2}-{}^4I_{11/2}$ (at $\sim 978 \text{ nm}$) and ${}^4I_{15/2}-{}^4I_{9/2}$ (at $\sim 800 \text{ nm}$) that can be excited with semiconductor lasers, yielding blue, green, and red emissions. The efficiency of the UC depends on many factors, such as the spatial distribution of the dopants and the phonon energy of the matrix. Increasing the dopant concentration can result in increased upconversion efficiency.¹³ But too high dopant concentration will decrease the upconversion efficiency because of cross relaxation between doped ions.¹⁴ Codoping with Yb^{3+} has proven to be a successful alternative for the upconversion process, which has a much larger absorption cross section than Er^{3+} near

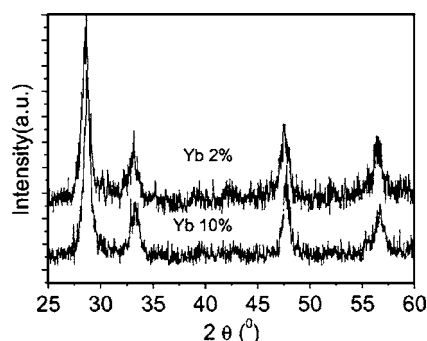
978 nm. There is a large spectral overlap between the ${}^2F_{5/2}-{}^2F_{7/2}$ Yb^{3+} NIR emission and the ${}^4I_{11/2}-{}^4I_{15/2}$ Er^{3+} absorption bands, which result in an efficient energy transfer (ET).

In this paper, we report the preparation and UCL properties of $\text{Gd}_2\text{O}_3:\text{Yb}^{3+}, \text{Er}^{3+}$ nanowires (NWs), especially the influence of Yb^{3+} codoping on UCL process of Er^{3+} . It was observed that the luminescent properties of RE ions depended not only on the size of NCs, but also on the dimension of them.¹⁵⁻¹⁷ To our knowledge, the UCL properties of RE ions in one-dimensional NWs have not been studied until now, despite those in zero-dimensional nanoparticles which have been widely studied.^{18,19}

II. EXPERIMENTS

Cubic Gd_2O_3 nanocrystallines doped with 1 mol % of Er_2O_3 and 2, 4, 8, and 10 mol % of Yb_2O_3 [$\text{Gd}_2\text{O}_3:\text{Er}^{3+}(1\%)$, $\text{Yb}^{3+}(2\%); \text{Gd}_2\text{O}_3:\text{Er}^{3+}(1\%)$, $\text{Yb}^{3+}(4\%); \text{Gd}_2\text{O}_3:\text{Er}^{3+}(1\%)$, $\text{Yb}^{3+}(8\%); \text{Gd}_2\text{O}_3:\text{Er}^{3+}(1\%)$, $\text{Yb}^{3+}(10\%)$] were prepared using a hydrothermal synthesis procedure. The preparation of similar RE_2O_3 nanocrystalline was originally reported by Li and Wang.⁶ In our work, appropriate amounts of high-purity Gd_2O_3 and Yb_2O_3 and Er_2O_3 in molar ratios of 1.94:0.04:0.02, 1.90:0.08:0.02, 1.82:0.16:0.02, and 1.78:0.20:0.02 were dissolved into concentrated HNO_3 . Then appropriate volume dilute KOH solution was added to the nitrate solution to form $\text{Gd}(\text{OH})_3$. Diluted KOH solution (1M) was used to adjust the pH values of $\text{Gd}(\text{OH})_3$ solutions; the final pH value was 13. After well stirred, the milky colloid solution was obtained and poured into several closed Teflon-lined autoclaves. Then the colloid solution was heated at 130°C for 17 h. The obtained sus-

^{a)}Author to whom correspondence should be addressed. Fax: 86-431-6176320; Electronic mail: hwsong2005@yahoo.com.cn

FIG. 1. XRD patterns of $\text{Gd}_2\text{O}_3:\text{Er}^{3+}, \text{Yb}^{3+}$ nanocrystals.

pension was washed and dried at 50 °C at vacuum condition. The dried $\text{Gd}(\text{OH})_3$ powders were annealed at 500 °C for 1 h. Then the nanocrystalline $\text{Gd}_2\text{O}_3:\text{Er}^{3+}, \text{Yb}^{3+}$ powders were obtained. Crystal structure, morphology, and size were obtained by x-ray diffraction (XRD) using Cu target radiation resource ($\text{Cu } K\alpha = 1.54078 \text{ \AA}$) and transmission electron micrograph (TEM), respectively.

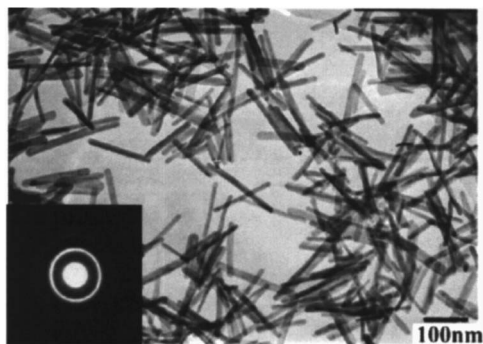
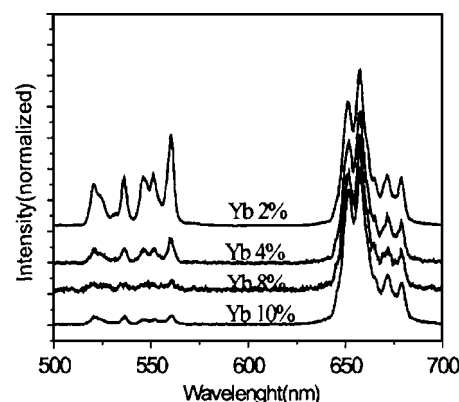
In the measurements of UCL emission spectra, a continuous 978-nm diode laser with power maximum of 2 W was used for excitation, with a focused area of 0.25 mm². The visible emissions were collected using an F-4500 spectrometer.

III. RESULTS AND DISCUSSION

A. Sample characterization

Figure 1 shows the XRD patterns of the $\text{Gd}_2\text{O}_3:\text{Yb}^{3+}, \text{Er}^{3+}$ powders. As shown, the powders yield pure cubic nanocrystalline. Estimated according to the widths of the XRD patterns by the Scherrer equation, the average crystalline size is $\sim 15 \text{ nm}$.

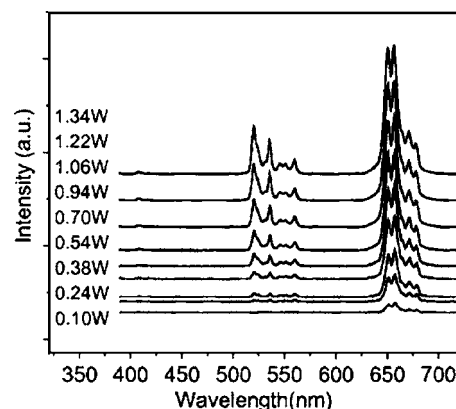
Figure 2 shows the TEM images of the $\text{Gd}_2\text{O}_3:\text{Yb}^{3+}, \text{Er}^{3+}$ powders. It is clear that all the nanocrystalline powders yield homogeneous NWs, with average diameters of 15–16 nm and lengths of 200–300 nm. Judged according to the inserted electron-diffraction patterns (EDPs), the NWs belong to multicrystals. Noted that as the doping concentration of Yb^{3+} ions varies, the XRD patterns hardly change, indicating that the structure and the crystalline size in different samples are same.

FIG. 2. TEM images of $\text{Gd}_2\text{O}_3:\text{Er}^{3+}, \text{Yb}^{3+}$ nanocrystals.FIG. 3. Upconversion luminescent spectra of various $\text{Gd}_2\text{O}_3:\text{Er}^{3+}(1\%), \text{Yb}^{3+}$ (2%, 4%, 8%, and 10%) nanowires under 978-nm excitation ($I_p = 0.96 \text{ W/mm}^2$).

B. UCL spectra of $\text{Gd}_2\text{O}_3:\text{Yb}^{3+}, \text{Er}^{3+}$ NWs

Figure 3 shows the UCL spectra of $\text{Gd}_2\text{O}_3:\text{Er}^{3+}, \text{Yb}^{3+}$ NWs with various concentrations of Yb^{3+} ions. In the spectra the green lines were observed between 500 and 580 nm, corresponding to the ${}^2H_{11/2}, {}^4S_{3/2} \rightarrow {}^4I_{15/2}$ transitions, while the red lines were observed between 640 and 690 nm, corresponding to the ${}^4F_{9/2} \rightarrow {}^4I_{15/2}$ transitions. Unlike those in $\text{Y}_2\text{O}_3:\text{Yb}^{3+}/\text{Er}^{3+}$ nanoparticles,¹⁹ the three-photon blue emissions of ${}^2H_{9/2} \rightarrow {}^4I_{15/2}$ were too weak to observe in $\text{Gd}_2\text{O}_3:\text{Yb}^{3+}, \text{Er}^{3+}$ NWs. It was seen that in $\text{Gd}_2\text{O}_3:\text{Yb}^{3+}, \text{Er}^{3+}$ NWs the relative intensity of red emissions to the green emissions increased with increasing Yb^{3+} concentration. Similar phenomenon was also observed in $\text{Y}_2\text{O}_3:\text{Yb}^{3+}/\text{Er}^{3+}$ nanoparticles.²⁰ Note that in $\text{Y}_2\text{O}_3:\text{Yb}^{3+}/\text{Er}^{3+}$ nanoparticles, the green emission was stronger than the red when the Yb^{3+} concentration was lower, while the red was stronger than the green when the Yb^{3+} concentration was higher. In the present $\text{Gd}_2\text{O}_3:\text{Yb}^{3+}, \text{Er}^{3+}$ NWs, the red emission is stronger than the green all the time.

Figure 4 shows the UCL spectra of $\text{Gd}_2\text{O}_3:\text{Er}^{3+}(1\%), \text{Yb}^{3+}(10\%)$ under the excitation with different powers. It is apparent that the intensity ratio of the green emission to the red emission increased with the in-

FIG. 4. Upconversion luminescent spectra of the $\text{Gd}_2\text{O}_3:\text{Er}^{3+}(1\%), \text{Yb}^{3+}(10\%)$ nanowires under the 978-nm excitation with different powers.

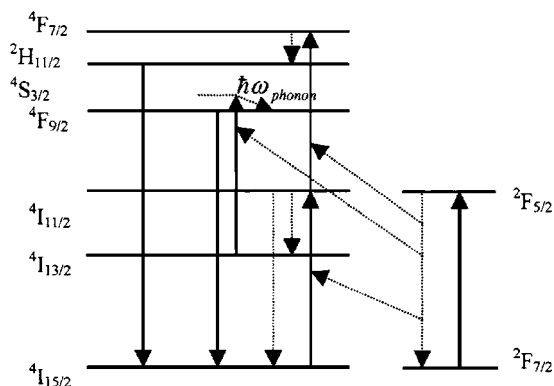


FIG. 5. Energy-level diagram of $\text{Er}^{3+}/\text{Yb}^{3+}$ -codoped nanocrystalline and UPL processes under 978 nm excitation.

creasing excitation power. Similar experiments were also performed in the other samples and the results were same.

C. Population and UCL processes

Figure 5 presents the energy-level diagram of $\text{Yb}^{3+}/\text{Er}^{3+}$ -codoped system and population processes under 978-nm excitation. In Er^{3+} - and Yb^{3+} -codoped systems, the upconversion occurs via two successive transfers of energy from the Yb^{3+} ion to the Er^{3+} ion.^{21,22} Following 978 nm irradiation, firstly, Er^{3+} ions in the ground states are excited to $^4I_{11/2}$ states via ET of neighboring Yb^{3+} and Er^{3+} . Subsequent nonradiative relaxations of $^4I_{11/2} \rightarrow ^4I_{13/2}$ also populate the $^4I_{13/2}$ levels.^{19,20} In the bulk Gd_2O_3 , the maximum of phonon energy is around 600 cm^{-1} , which is much smaller than the energy gaps of $^4I_{11/2}$ and $^4I_{13/2}$. According to the theory of multiphonon relaxation, the nonradiative relaxation probability of $^4I_{11/2} \rightarrow ^4I_{13/2}$ is relatively small.²³ In the present NCs, a large number of high-energy vibration modes such as OH^- and CO_3^{2-} bonds are involved owing to the high surface-to-volume ratio. Few high-energy phonons can easily bridge the gap between the $^4I_{11/2}$ and $^4I_{13/2}$ states and the probability of multiphonon relaxation is rather large. In the second-step excitation, the same laser pumps the excited-state atoms from the $^4I_{11/2}$ to the $^4F_{7/2}$ levels via ET and excited-state absorption (ESA), or from the $^4I_{13/2}$ to the $^4F_{9/2}$ states via phonon-assisted ET. Subsequent nonradiative relaxations of $^4F_{7/2} \rightarrow ^4S_{3/2}$ and $^4F_{7/2} \rightarrow ^4F_{9/2}$ populate the $^4S_{3/2}$ ($^2H_{11/2}$) as well as the $^4F_{9/2}$ states. As a consequence, the two-photon green emissions of $^4S_{3/2} \rightarrow ^2H_{11/2} \rightarrow ^4I_{15/2}$ and the red emissions of $^4F_{9/2} \rightarrow ^4I_{15/2}$ occur.

Note that the phonon-assisted ET of $^4S_{3/2}(\text{Er}^{3+}) + ^2F_{7/2}(\text{Yb}^{3+}) \rightarrow ^4I_{13/2}(\text{Er}^{3+}) + ^2F_{5/2}(\text{Yb}^{3+})$ happens, leading the green emission to the decrease, while the red to increase with increasing the Yb^{3+} concentration. The evidence was given in one of our previous papers.¹⁹ Actually, the thermal effect may also lead the quenching of the green emission and the enhancement of the red due to the improved nonradiative relaxation, which will be discussed in detail in the Sec. III E.

D. Power dependence of UCL and saturation effect

To better understand the mechanism by which the $^2H_{11/2}$, $^4S_{3/2}$ and $^4F_{9/2}$ excited states are populated following NIR

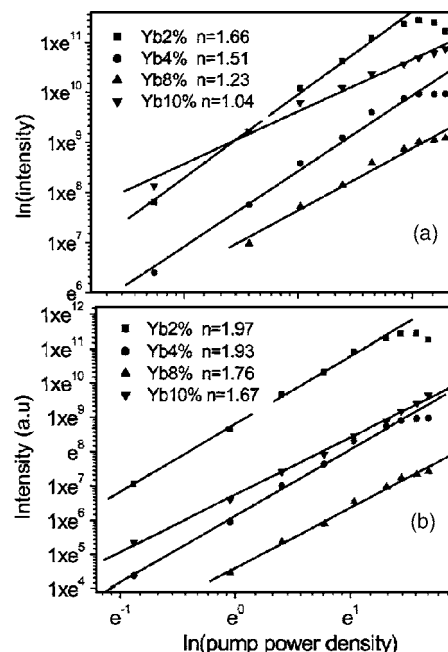


FIG. 6. In-In plot of emission intensity as a function of excitation power, (a) the red emission, and (b) the green emission.

irradiation, the UCL intensity of the green ($^2H_{11/2}$, $^4S_{3/2} \rightarrow ^4I_{15/2}$) and red ($^4F_{9/2} \rightarrow ^4I_{15/2}$) emissions as a function of the excitation power was studied. Figures 6(a) and 6(b) show the In-In plot of the emission intensity as a function of excitation power, for the green and the red emissions, respectively. It can be seen that as the pump power (I_p) was lower than $\sim 1 \text{ W}$, the emission intensity (I_{UCL}) increased with I_p obeying a rule of $I_{\text{UCL}} \propto I_p^n$, for both the green and the red emissions. Moreover, the slope (n) in the In-In plot varied with the Yb^{3+} concentration. For the green emission, the values of n were determined to be 1.97, 1.93, 1.76, and 1.67, respectively, in $\text{Gd}_2\text{O}_3:\text{Er}^{3+}(1\%), \text{Yb}^{3+}(2\%)$; $\text{Gd}_2\text{O}_3:\text{Er}^{3+}(1\%), \text{Yb}^{3+}(4\%)$; $\text{Gd}_2\text{O}_3:\text{Er}^{3+}(1\%), \text{Yb}^{3+}(8\%)$; and $\text{Gd}_2\text{O}_3:\text{Er}^{3+}(1\%), \text{Yb}^{3+}(10\%)$. For the red, the values of n were determined to be 0.66, 1.51, 1.23, and 1.04, respectively, in $\text{Gd}_2\text{O}_3:\text{Er}^{3+}(1\%), \text{Yb}^{3+}(2\%)$; $\text{Gd}_2\text{O}_3:\text{Er}^{3+}(1\%), \text{Yb}^{3+}(4\%)$; $\text{Gd}_2\text{O}_3:\text{Er}^{3+}(1\%), \text{Yb}^{3+}(8\%)$; and $\text{Gd}_2\text{O}_3:\text{Er}^{3+}(1\%), \text{Yb}^{3+}(10\%)$. Apparently, the value of n decreased with increasing the Yb^{3+} concentration in the range of 1–2. It can be also seen that as the power surpassed 1 W, I_{UCL} tended to decrease.

As is well known, for any upconversion mechanism, the value of n presents the number of IR photons absorbed per visible photon emitted.^{24,25} For the two-photon processes, n should equal/close to 2. However, the values of n were close to 1 for the red emission. This was mainly attributed to the competition between linear decay and upconversion processes for the depletion of the intermediate excited states, which was theoretically described by Pollnau *et al.*²⁴ In Ref. 24, considering on a three-level system with levels of $|0\rangle$, $|1\rangle$, and $|2\rangle$ (the ground state, the intermediate level, and the UCL level) and assuming that the populating from $|0\rangle$ to $|1\rangle$ is a ground-state absorption (GSA) process and from $|1\rangle$ and $|2\rangle$ is an ESA or ET process, the authors deduced that I_{UCL} was proportional to I_p^2 when the linear decay of the intermediate

state was the dominant depletion mechanism of $|1\rangle$, while I_{UCL} was proportional to I_p when the upconversion was the dominant mechanism.

In the present $\text{Er}^{3+}/\text{Yb}^{3+}$ -codoped materials, the mechanism of UCL is different from that described in Ref. 24. Here, considering on a similar three-level system and assuming that the UCL processes are two-step ET ones between neighboring Er^{3+} and Yb^{3+} ions, the steady-state luminescent rate equations can be written as

$$W_0 N_0 N_{\text{Yb}1} - W_1 N_1 N_{\text{Yb}1} - A_1 N_1 = 0, \quad (1)$$

$$W_1 N_1 N_{\text{Yb}1} - A_2 N_2 = 0, \quad (2)$$

$$\rho_p \sigma N_{\text{Yb}0} - (W_0 N_0 + W_1 N_1) N_{\text{Yb}1} - B_1 N_{\text{Yb}1} = 0, \quad (3)$$

with

$$\rho_p = \frac{\lambda_p}{hc\pi w_p^2} I_p, \quad (4)$$

where N_0 and N_1 and N_2 , $N_{\text{Yb}0}$, and $N_{\text{Yb}1}$ are populations of $|0\rangle$, $|1\rangle$, and $|2\rangle$ ground-state Yb^{3+} and excited-state Yb^{3+} , respectively, A_1 and A_2 and B_1 are decay rates of $|1\rangle$ and $|2\rangle$ and the excited state of Yb^{3+} , respectively, W_0 and W_1 are ET rates for the first step and the second step, respectively, λ_p is the pump wavelength, w_p is the pump radius, h is Planck's constant, and c is the vacuum speed of light. Due to $N_0 \ll N_1$, based on Eq. (4) we have

$$N_{\text{Yb}1} = \rho_p \sigma N_{\text{Yb}0} / (W_0 N_0 + B_1). \quad (5)$$

If the linear decay is the dominant depletion mechanism of level 1, we can neglect the upconversion term in Eq. (2). Then we can deduce that

$$N_1 = \frac{W_0 N_0}{A_1} \frac{\sigma_0 N_{\text{Yb}0}}{W_0 N_0 + B} \rho_p, \quad (6)$$

$$N_2 = \frac{W_0 W_1 N_0}{A_1 A_2} \left(\frac{\sigma_0 N_{\text{Yb}0}}{W_0 N_0 + B} \right)^2 \rho_p^2. \quad (7)$$

In contrast, if the upconversion is dominant, we neglect the linear decay term in Eq. (2), then obtain that

$$N_1 = \frac{W_0 N_0}{W_1}, \quad (8)$$

$$N_2 = \frac{W_0 W_1 N_0}{A_1 A_2} \left(\frac{\sigma_0 N_{\text{Yb}0}}{W_0 N_0 + B} \right) \rho_p. \quad (9)$$

Obviously, if the linear decay is dominant, $N_2 \propto I_p^2$. If the upconversion is dominant, $N_2 \propto I_p$. This result is similar with that deduced in Ref. 24, despite the UCL mechanism is different.

As the Yb^{3+} concentration increases, the ET from Yb^{3+} to Er^{3+} will make upconversion from $|1\rangle$ to $|2\rangle$ more effective, resulting in increasing importance of upconversion. As a consequence, the slope of the UCL varies from quadratic to linear.²⁴ As mentioned above, the slopes of the green emission are nearly 2, while the slopes of red emissions are close to 1. This can be attributed to the difference of the intermediate level between the green and the red emissions. The

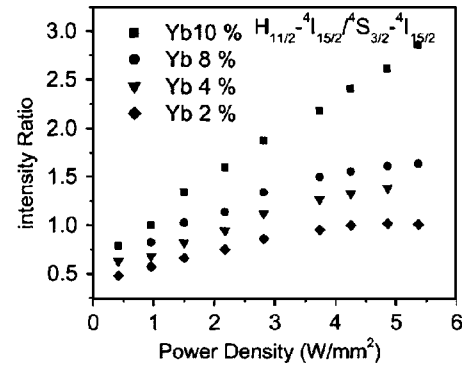


FIG. 7. Intensity ratio of ${}^2H_{11/2}$ - ${}^4I_{15/2}$ to ${}^4S_{3/2}$ - ${}^4I_{15/2}$ as a function of excitation power in different samples.

intermediate level of the green emission is ${}^4I_{11/2}$. Because of the nonradiative relaxation of ${}^4I_{11/2}$ - ${}^4I_{13/2}$, which contributes considerably to the linear decay of ${}^4I_{13/2}$, the relative importance of upconversion is decreased, leading the slope of the green emission to be ~ 2 . The intermediate level of the red emission is ${}^4I_{13/2}$, which has a relatively small downconversion decay rate. The upconversion is the dominant depletion mechanism of ${}^4I_{13/2}$, thus the slope of the green emission is close to 1.

Note that the competition between linear decay and upconversion processes for the depletion of the intermediate excited states cannot well explain the fact that I_{UCL} decreases with increasing I_p as it is more than 1 W. Actually, this can be attributed to thermal quenching of UCL caused by the exposure of the 978-nm light. In the next section, we will demonstrate that with the increase of the Yb^{3+} concentration and excitation power, the sample temperature at the irradiated spot increases remarkably. The temperature increase will lead to the quenching of UCL and also to the variation of the slope of UCL.

E. Thermal effect

In nanometer materials, the electron-phonon interaction becomes much stronger than that in the bulk. The thermal effect caused by the exposure of the 978-nm diode laser has to be considered. For Er^{3+} ions, the energy separation between the two nearest excited states ${}^2H_{11/2}$ and ${}^4S_{3/2}$ is only

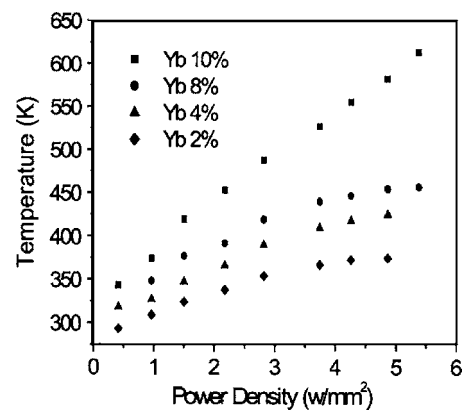


FIG. 8. Practical sample temperature at the exposure spot as a function of excitation power in different samples.

several hundred wave numbers. As the down $^4S_{3/2}$ level is populated, immediately the upper $^2H_{11/2}$ level is thermal populated owing to Boltzmann's distribution. This will lead the intensity ratio (R_{HS}) of $^2H_{11/2}$ - $^4I_{15/2}$ to $^4S_{3/2}$ - $^4I_{15/2}$ to be sensitive to temperature. Therefore, R_{HS} is a critical parameter to study thermal effect in $Gd_2O_3:Yb^{3+},Er^{3+}$ NWS under the exposure of the 978-nm diode laser. Figure 8 shows R_H as a function of temperature in different samples. It is obvious that the higher the Yb^{3+} concentration was and the stronger excitation power was, the larger the value of R_H was. When the Yb^{3+} -ion concentration or the excitation power increased, more 978-nm photons were absorbed, leading the temperature to increase more. According to Boltzmann's distribution, R_{HS} as a function of temperature can be written as

$$R_{HS} = R_{HS}(0)\exp(-\Delta E/kT), \quad (10)$$

where $R_{HS}(0)$ is a constant, ΔE is the energy separation between the $^2H_{11/2}$ and the $^4S_{3/2}$ levels ($\sim 700\text{ cm}^{-1}$), k is Boltzmann's constant, and T is the absolute temperature. As the excitation power and Yb^{3+} concentration was lower, the sample temperature at the pumped spot should be close to room temperature ($\sim 293\text{ K}$), corresponding to $R_{HS}=0.48$. Considering this fact, $R_{HS}(0)$ was chosen to be 16. Based on the experimental relationship of R_{HS} and I_P and the calculated relationship of R_{HS} and T , the temperature at the irradiated spot (T_{IR}) as a function of pump power can be deduced, as drawn in Fig. 7. In $Gd_2O_3:Er^{3+}(1\%),Yb^{3+}(2\%)$ NWs, the temperature increased $\sim 80\text{ K}$ as the excitation power density varied from 0.4 to 4.88 W/mm^2 . In $Gd_2O_3:Er^{3+}(1\%),Yb^{3+}(10\%)$ NWs, the temperature increased as high as $\sim 250\text{ K}$ as the excitation power density varied from 0.4 to 4.88 W/mm^2 . In $Gd_2O_3:Er^{3+},Yb^{3+}$ nanocrystals, owing to the involving of numerous surface defects with high phonon energy, such as OH^- bonds, the electron-phonon interaction becomes stronger. As a consequence, the thermal effect has to be considered.

IV. CONCLUSIONS

The UCL in $Gd_2O_3:Er^{3+}/Yb^{3+}$ NWs was studied under 978-nm excitation. The results indicated that the relative intensity of the red emission ($^4F_{9/2}$ - $^4I_{15/2}$) increased with increasing the Yb^{3+} concentration, while that of the green emission ($^4S_{3/2}$ - $^2H_{11/2}$ - $^4I_{15/2}$) decreased. The intensity saturation phenomenon caused by competition between linear decay and upconversion processes for the depletion of the intermediate excited states was observed in $Gd_2O_3:Er^{3+}/Yb^{3+}$

NWs. This phenomenon depended strongly on the Yb^{3+} concentration and population paths. The thermal effect caused by 978-nm diode laser irradiation was studied according to the intensity ratio of $^2H_{11/2}$ - $^4I_{15/2}$ to $^4S_{3/2}$ - $^4I_{15/2}$. The result demonstrated that in $Gd_2O_3:Er^{3+},Yb^{3+}$ nanocrystals, the practical temperature at the irradiated spot considerably increased owing to the increased electron-phonon interaction in comparison to the bulk materials.

ACKNOWLEDGMENTS

The author gratefully thanks National Natural Science Foundation of China (Grant No. 10374086) and Talent Youth Foundation of JiLin Province (Grant No. 20040105).

- ¹H. Eilers and B. M. Tissue, Chem. Phys. Lett. **251**, 74 (1996).
- ²R. N. Bhargava, J. Lumin. **72-74**, 46 (1997).
- ³J. A. Capobianco, F. Vetrone, T. D. Alesio, G. Tessari, A. Speghini, and M. Bettinelli, Phys. Chem. Chem. Phys. **2**, 3203 (2000).
- ⁴E. Zych, D. Hreniak, and W. Strek, J. Phys. Chem. B **106**, 3805 (2002).
- ⁵Y. L. Soo, S. M. Huang, Z. H. Ming, Y. H. Kao, G. C. Smith, E. Goldburt, R. Hodel, B. Kulkarni, J. V. D. Veladias, and R. N. Bhargava, J. Appl. Phys. **83**, 5404 (1998).
- ⁶Y. Li and X. Wang, Chem.-Eur. J. **9**, 5627 (2003).
- ⁷Y. Sun, B. Gates, B. Mayers, and Y. Xia, Nano Lett. **2**, 165 (2002).
- ⁸X. Wang, X. Sun, D. Yu, B. Zou, and Y. Li, Adv. Mater. (Weinheim, Ger.) **15**, 1442 (2003).
- ⁹S. Shen and K. Hidajat, Adv. Mater. (Weinheim, Ger.) **16**, 54 (2004).
- ¹⁰M. P. Hehlen, G. Frei, and H. U. Güdel, Phys. Rev. B **50**, 16264 (1994).
- ¹¹T. Riedener, P. Egger, J. Hulliger, and H. U. Güdel, Phys. Rev. B **56**, 1800 (1997).
- ¹²R. Balda, A. J. Garcia-Adeva, M. Voda, and J. Fernandez, Phys. Rev. B **69**, 205203 (2004).
- ¹³P. Goldner and F. Pellé, J. Lumin. **83-84**, 297 (1999).
- ¹⁴G. M. Salley, R. Valiente, and H. U. Güdel, J. Lumin. **94-95**, 305 (2001).
- ¹⁵H. Song, L. Yu, S. Lu, T. Wang, Z. Liu, and L. Yang, Appl. Phys. Lett. **85**, 470 (2004).
- ¹⁶L. Yu, H. Song, S. Lu, Z. Liu, L. Yang, and X. Kong, J. Phys. Chem. B **108**, 16697 (2004).
- ¹⁷L. Yu, H. Song, S. Lu, Z. Liu, and L. Yang, Chem. Phys. Lett. **399**, 384 (2004).
- ¹⁸J. Capobianco, F. Vetrone, J. C. Boyer, A. Speghini, and M. Bettinelli, J. Phys. Chem. B **106**, 1181 (2002).
- ¹⁹H. Song, B. Sun, T. Wang, S. Lu, L. Yang, B. Chen, X. Wang, and X. Kong, Solid State Commun. **132**, 409 (2004).
- ²⁰F. Vetrone, J. C. Boyer, and J. A. Capobianco, J. Appl. Phys. **96**, 661 (2004).
- ²¹F. Auzel, C. R. Acad. Sci. (Paris) **262**, 1016 (1966).
- ²²L. F. Johnson, H. G. Guggenheim, T. C. Rich, and F. W. Ostermayer, J. Appl. Phys. **43**, 1125 (1972).
- ²³C. B. Layne, W. H. Lowdermilk, and M. J. Weber, Phys. Rev. B **16**, 10 (1977).
- ²⁴M. Pollnau, D. R. Gamelin, S. R. Lüthi, H. U. Güdel, and M. P. Hehlen, Phys. Rev. B **61**, 3337 (2000).
- ²⁵M. A. Chamorro and R. Cases, J. Lumin. **46**, 59 (1990).